Correlation between Ionic Conductivity and Mechanical Properties of Solid-like PEO Polymer Electrolyte

Agathe Naboulsi, Ronan Chometon, François Ribot, Giao Nguyen, Odile Fichet, Christel Laberty-Robert

Correlation between Ionic Conductivity and Mechanical Properties of Solid-like PEO Polymer Electrolyte

Agathe Naboulsi,[1,2,3] Ronan Chometon,[2,3,4] François Ribot,[2] Giao Nguyen,[1] Odile Fichet[1], Christel Laberty-Robert,[2,3]

[1] CY Cergy Paris Université, LPPI, F-95000 Cergy, France

[2] Sorbonne Université, CNRS, Laboratoire Chimie de la Matière Condensée de Paris, LCMCP, 4 Place Jussieu, 75005 Paris, France

[3] RS2E, Réseau Français sur le Stockage Electrochimique de l'Energie, CNRS 3459, 80039 Cedex 1 Amiens, France

[4] CSE, Collège de France, 4 Place Marcellin Berthelot, 75005 Paris, France

Abstract

Poly (ethylene oxide) (PEO) networks, with or without anionic bis(trifluoromethanesulfonyl)imide (TFSI) grafted groups, are promising electrolytes for Li-metal all solid-state batteries. Nevertheless, there is need to enhance our current understanding of the physico-chemical characteristics of these polymer networks to meet the mechanical and ionic conductivity property requirements for Li battery electrolyte materials. To address this challenge, our goal is to investigate the impact of the crosslinking density of the PEO network and the ethylene oxide/lithium ratio on mechanical properties (such as glass transition temperature and storage modulus) and ionic conductivity. We have synthesized a series of cross-linked PEO polymers (si-SPE for single ion Solid Polymer Electrolyte) via solvent-free radical copolymerization. These polymers are synthesized by using commercially available lithium 3-[(trifluoromethane)sulfonamidosulfonyl]propyl methacrylate (LiMTFSI), Poly(ethylene glycol)methylether methacrylate (PEGM) and (poly(ethylene glycol) dimethacrylate) (PEGDM). In addition, we have synthesized a series of cross-linked PEO polymers (SPE for Solid Polymer Electrolyte) using LiTFSI, as the ionic species. Most of the resulting polymer films are amorphous, self-standing, flexible, homogenous, and thermally stable. Interestingly, our research has revealed a correlation between ionic conductivity and mechanical properties in both SPE and si-SPE series. Ionic conductivity increases as glass transition temperature, α relaxation temperature, and storage modulus decrease, suggesting that Li^+ transport is influenced by polymer chain flexibility and Li^+/EO interaction.

Keywords

Cross-linked polymer network – Solid Polymer Electrolyte – Single ion conductor – Transport number – Mechanical properties

1. Introduction

The growing demand for portable energy storage is driving researchers to improve battery storage capacity. With lithium-ion technology approaching its capacity limits, scientists are dedicating their research efforts to the development of the next generation of lithium batteries.[1] Lithium metal is a preferred choice for anodes due to its high theoretical capacity, but it faces security concerns primarily related to the formation of dendrites. These dendrites result from the irregular deposition of metallic lithium, potentially induced by the formation of the solid electrolyte interphase (SEI) layer, coming from the contact of Li-metal with organic liquid electrolyte[2,3]. On the other hand, polymer-based Solid-State Batteries (SSBs) have attracted great attention in recent years due to their enhanced safety over conventional liquid electrolytes in terms of electrolyte leakage, wide operation temperature, and dendrite growth[3–5]. In these systems, the classical polymer electrolyte is based on polyethylene oxide (PEO), due to its excellent capability to dissolve Li-salts, thanks to the complexation of Li^+ with ethylene oxide sites and its interesting ionic conductivity yet at relative high temperatures (> 60 °C). More specifically, the PEO/lithium bis(trifluoromethanesulfonyl) imide (LiTFSI) system has been widely studied because of the high dissociation and plasticizing capabilities of LiTFSI, which lead to better ionic conductivities compared to other salts[6,7]. However, the high crystallinity and the low mechanical strength of PEO are still issues to be improved[8]. Specifically, its crystallization at ambient temperature limits its ionic conductivity, due to the reduction of amorphous conductivity pathways caused by the spherulitic growth[9].

Many strategies have been explored to enhance the ionic conductivity of solid polymer electrolyte (SPE) based on PEO (Table 1).

Among these strategies, the addition of a plasticizer into PEO matrix plays a crucial role in suppressing its crystallinity and reducing the ion-pairing of the Li-salt, ultimately increasing ionic mobility. Aprotic organic solvent and low molecular weight PEO have also been incorporated into the PEO-LiX matrices. While achieving an ionic conductivity value of 10^{-4} S.cm^{-1} at room temperature, it is worth noting that the inclusion of a liquid plasticizer can lead to a loss of mechanical properties. Interestingly, the introduction of propylene carbonate and ethylene carbonate improved ionic conductivity, but unexpectedly reduced the Li transport number of the plasticized polymer electrolyte[10]. An alternative approach focuses on increasing the oxygen ether sites to raise matrix polarity and, in turn, improve ionic mobility.[11] Balsara's group has extensively explored this strategy through the synthesis of poly(1,3,6-trioxocane) (P(2EO-MO)), a polyether consisting of two ethylene oxide and one methylene oxide units[11,12]. The resulting solid polymer electrolyte (SPE) with LiTFSI exhibited lower ionic conductivity compared to PEO-based electrolytes. However, it displayed an improvement in Li transport number, increasing from 0.08 to 0.2. Furthermore, blending P(2EO-MO) with PEO resulted in a new matrix for SPE, although it exhibited similar ionic transport properties to the conventional PEO matrix. Despite

these efforts, the best-reported ionic conductivity remains around 10^{-4} $S.cm^{-1}$, even at elevated temperatures such as 60 °C.

Table 1. Main characteristics of PEO-based SPEs and si-SPE reported in the literature.

PEO-based polymer matrix	Additive/ Solvent	Ionic conductivity ($S.cm^{-1}$)	Electrochemical windows	t^+ Transport number	Authors/Ref
Linear polymer					
Linear PEO	LiTFSI	10^{-3}@60°C		0.15-0.44 @90°C	Devaux and al.[13]
Polymer blend					
PEO-P(2EO-MO) poly- (1,3,6-trioxocane)	LiTFSI/ THF	10^{-3} @90°C		0.08 to 0.2 @90°C	Gao and al.[12]
Blend of PEO–PFSILi lithiated poly(perfluoroalkylsulfonyl)imide	MeCN	$2x10^{-4}$@80°C	0-5.5V	0.9	Shi and al.[14]
Phenylsulfonyl(trifluoromethylsulfonyl)imide lithium salt / PEO	MeCN/H_2O	$2x10^{-4}$@90°C		0.90-0.92 @90°C	Nguyen and al.[15]
LiPSsTFSI-PEO poly[(4-styrenesulfonyl) TFSI]	DMF	$1x10^{-4}$@90°C	0-4.5V	0.91@60°C	Ma and al.[6]
Copolymer					
combPEO Polystyrene-b-PEO comb	LiTFSI/ CH_2Cl/MeCN	10^{-4} @60°C	0-4.5V	0.15@90°C	Devaux and al.[16]
P(STFSILi)-b-PEO-b-P(STFSILi)	Dioxane	$1x10^{-5}$@60°C	0-6.5V	0.85@90°C	Bouchet and al.[2]
Li[PSTFSI-*co*-MPEGA]	DMF or MeOH	$8x10^{-6}$@25°C		0.94@60°C	Feng and al.[17]
PS-*b*-P(MALi-*co*-OEGMA) poly(lithium methacrylate-co-oligoethylene glycol methacrylate)	THF/MeOH	$2x10^{-5}$@20°C	0-5V	0.84@90°C	Rolland and al.[18]
PEO–PSLiTFSI	DMF	$3x10^{-8}$@25°C		0.95@90°C	Inceoglu and al.[19]
poly(PEGM)-*b*-poly(LiMTFSI)	DMF	$2x10^{-6}$@25°C	0-4.5V	0.83@70°C	Porcarelli and al.[20]
PMATFSI-b-PEO-b-PMATFSI	Dioxane	$3x10^{-6}$@60°C	0-4V	0.8-0.92 @90°C	Devaux and al.[21]
Network					
PEGM-PEGDM	LiTFSI/PC	$2x10^{-3}$@25°C		0.14@70°C	Lechartier and al.[22]
PEGM-PEGDM-LiMTFSI	PC	$1x10^{-4}$@25°C	0-5.5V	0.89-0.91 @70°C	Porcarelli and al.[23]
PEGM-PEGDM-LiMTFSI	PC	$5x10^{-5}$@25°C		0.73@60°C	Lechartier and al.[22]
Lithium poly (bisphenol A borate) / PEO	MeCN	$2x10^{-7}$@25°C	0-5.5V	0.92@60°C	Zhang and al.[24]
Lithiated mimic neurons in PEGMA	Acetone	$1x10^{-4}$@25°C		0.974	Li and al.[25]

Nanostructured block copolymer electrolytes (BCEs)[2,26–28], often incorporating PEO blocks, have been suggested as a mean to improve the mechanical properties of SPE, typically at elevated temperatures beyond the melting temperature of PEO. For instance, Bouchet *et al.*[16] have designed a large number of BCEs based on either 1/ linear polyethylene oxide (PEO) or 2/ combination of PEO as the ionic conductor block, and poly(styrene) as the structural block (combPEO), using LiTFSI as electrolyte. The authors concluded that combPEO blocks allow the suppression of PEO crystallization and mechanical properties of the BCEs depend only on the molecular weight (M_n) and the volume fraction of the polystyrene block. Finally, these self-standing BCEs were obtained with a typical ionic conductivity of PEO/LiTFSI systems, ca. 10^{-4} S.cm^{-1} at 60 °C for the optimized design. Interestingly, high-concentration solid electrolytes (SEs) with a ratio of EO:$Li^+ \leq 6:1$ are developed using concentrated-salt chemistry. This strategy allows the use of this polymer at elevated oxidation potentials (>5 V vs. Li/Li^+) and they have found an increase of the oxidation potential with the degree of coordinated EO. [29]

To obtain self-standing and highly conducting SPE at room temperature, Mecerreyes *et al.*[23] have reported the synthesis of single-ion conducting polymer electrolyte gel via an in situ radical copolymerization of the (LiMTFSI), (PEGM), (PEGDM~~)~~ in the presence of propylene carbonate (PC). These self-standing materials showed a combination of high Li transport number (0.86 ± 0.02 @25 °C) and high ionic conductivity at ambient temperature ($\sigma \approx 10^{-4}$ S.cm^{-1}) but required the presence of carbonate solvent. Another strategy to increase ionic conductivity is to design composite electrolyte to eliminate the crystallinity of the PEO-like network.[30] In contrast to the aforementioned approach, our paper pursues a different strategy.

In these diverse studies, materials are predominantly characterized by their ionic conductivity, frequently assessed at various temperatures, thereby complexifying direct comparisons. Transport numbers and the potential stability range of the materials are rarely addressed. Additionally, there is minimal investigation of the mechanical properties. Consequently, the correlations between these distinct properties are rarely investigated.

The present work reports a simple design of SPE combining (i) PEO network for both self-standing characteristics and PEO crystallization suppression with (ii) LiMTFSI monomer for single-ion conducting properties. A systematic investigation on the effects of the crosslinking density of the PEO network and ~~of~~ the ethylene oxide/lithium (EO/Li) ratio on the glass transition temperature (T_g), storage modulus (E') and the ionic conductivity of electrolyte materials has been carried out. PEGM and PEGDM were selected as precursors of PEO networks because they are liquid and allow a solvent-free synthesis. The variation of the proportions between the two precursors allows modifying the crosslinking density. The EO/Li ratio was modulated by dissolving different amounts of methacrylate salts (LiMTFSI) in the PEGDM/PEGM mixtures with which they were then copolymerized to graft the anion on the PEO network. The Li transport numbers and the electrochemical stability window of the most promising materials were then evaluated. All these properties were systematically compared with those

of the polymer network with un-grafted anions, synthesized by replacing methacrylate salt ~~by~~ with LiTFSI additive.

2. Experimental

2.1. Materials

Poly(ethylene glycol) methyl ether methacrylate (PEGM, $M_n = 500$ g.mol^{-1}, Sigma Aldrich), poly(ethylene glycol) dimethacrylate (PEGDM, M_n=750 g.mol^{-1}, Sigma Aldrich) and lithium 3-[(trifluoromethane)sulfonamidosulfonyl]propyl methacrylate (LiMTFSI, Specific Polymer) were used as received. 2,2′-azobis(2-methylpropionitrile) (AIBN, initiator, 98%, Sigma Aldrich) was recrystallized in methanol before used. Bis(trifluoromethylsulfonyl) amine lithium salt (LiTFSI, > 99%, Sigma Aldrich) and lithium metal (99.9% Sigma Aldrich) were kept in the glove box (H_2O < 0.1 ppm).

2.2. Material synthesis

Single-ion solid polymer electrolyte (si-SPE) synthesis: PEGM, PEGDM and LiMTFSI were introduced in a vial according to the desired proportions (Table 2) and stirred at room temperature until LiMTFSI was completely dissolved (2 h). 2% wt of AIBN was added to the mixture, which was then degassed and flushed with nitrogen until the AIBN was dissolved (2-3 h). The mixture was poured into a mold made with two glass plates separated by a Teflon gasket. The gasket thickness was 125 µm or 500 µm. The molds were then placed in an oven at 70 °C for 2 h and then at 90 °C for 1h. The resulting polymer membranes were dried under vacuum (10-15 mbar) at 70 °C in a glass oven (BUCHI B-585) for 12 h. The membranes were kept in a glove box (at ambient temperature and H_2O < 0.1 ppm) until their characterization.

(SPE) synthesis: PEGM, PEGDM and AIBN were introduced in a vial at the desired quantities (Table 2). The vial was then placed in a glove box (H_2O < 0.1 ppm) and the required amount of LiTFSI was added to the mixture. The mixture was stirred until the LiTFSI was dissolved (1 h). The SPE membranes were synthesized using the same mold, the same synthesis and storage protocol as those for the si-SPE. The samples were named respectively as si–$SPE_{x.y}$ and $SPE_{x.y}$, where *x* is the LiMTFSI or LiTFSI weight proportion in the material and *y* is the PEGDM weight proportion. The 80:20 PEGM:PEGDM ratio without LiMTFSI or LiTFSI was used as the reference and was noted pristine (Table 2).

Table 2. Sample Compositions and main characteristics of $SPE_{x.y}$ and si-$SPE_{x.y}$ polymer electrolyte.

Sample	LiTFSI	LiMTFSI	PEGM	PEGDM	PEGM: PEGDM	[EO]/Li	[Li] (10^{-4} mol/g)	Tg (°C) ± 4°C	Soluble fraction (%wt)	Appearance	Conductivity (S/cm) at 25°C
PRISTINE	-	-	80	20	80:20	-	-	-60	2	flexible	7×10^{-10}
						SPE					
$SPE_{5.19}$	5	-	76	19	80:20	99	1.7	-55	5	flexible	$2\times10^{-6} \pm 1\times10^{-6}$
$SPE_{6.19}$	6	-	75	19	80:20	82	2.1	-54	7	flexible	$5\times10^{-6} \pm 1\times10^{-6}$
$SPE_{10.18}$	10	-	72	18	80:20	47	3.5	-55	11	flexible	$5\times10^{-6} \pm 2\times10^{-6}$
$SPE_{18.16}$	18	-	66	16	80:20	24	6.3	-56	21	flexible	$1\times10^{-5} \pm 3\times10^{-6}$
$SPE_{34.13}$	34	-	53	13	80:20	10	11.8	-42	32	flexible	$3\times10^{-6} \pm 1\times10^{-6}$
$SPE_{18.0}$	18	-	82	0	100:0	24	6.3	-52	17	gel	2×10^{-5}
$SPE_{18.4}$	18	-	78	4	95:5	24	6.3	-54	16	difficult to handle	$1\times10^{-5} \pm 3\times10^{-6}$
$SPE_{18.41}$	18	-	41	41	50:50	24	6.3	-40	17	hard	3×10^{-6}
$SPE_{18.82}$	18	-	0	82	0:100	24	6.3	-31	19	hard	2×10^{-7}
						si-SPE					
si-$SPE_{5.19}$	-	5	76	19	80:20	119	1.4	-52	2	flexible	$2\times10^{-7} \pm 1\times10^{-7}$
si-$SPE_{7.19}$	-	7	74	19	80:20	83	2.0	-53	3	flexible	$2\times10^{-7} \pm 5\times10^{-8}$
si-$SPE_{11.18}$	-	11	71	18	80:20	51	3.2	-50	3	flexible	$2\times10^{-7} \pm 1\times10^{-7}$
si-$SPE_{21.16}$	-	21	63	16	80:20	24	6.1	-41	2	flexible	$2\times10^{-7} \pm 9\times10^{-8}$
si-$SPE_{40.12}$	-	40	48	12	80:20	9	11.6	-29	6	flexible	$4\times10^{-9} \pm 1\times10^{-9}$
si-$SPE_{21.0}$	-	21	79	0	100:0	24	6.1	-40	7	gel	4×10^{-7}
si-$SPE_{21.4}$	-	21	75	4	95:5	24	6.1	-46	2	difficult to handle	4×10^{-7}
si-$SPE_{21.40}$	-	21	39.5	39.5	50:50	24	6.1	-39	1	hard	3×10^{-8}
si-$SPE_{21.48}$	-	21	31.5	47.5	40:60	24	6.1	-33	4	hard	4×10^{-8}
si-$SPE_{21.79}$	-	21	0	79	0:100	24	6.1	-19	2	hard	2×10^{-8}

2.3. Characterization

The soluble fraction of the different materials was quantified by solid/liquid extraction of a known weight (W_0) sample with an automated Soxhlet extractor BUCHI SPEED-EXTRACTOR E-914 and methanol as extraction solvent. For extraction, 3 cycles of 10 min were carried out at 80 °C under 100 bars. After extraction, the samples were dried under vacuum (10-15 mbar) at 60 °C until constant weight and then weighted (W_e). The soluble fraction was calculated as follows:

$$\%\ \text{soluble fraction} = \frac{W_0 - W_E}{W_0} * 100 \qquad \text{Equation 1}$$

Differential Scanning Calorimetry (DSC) measurements were performed on a DSC Q20 (TA Instruments). Samples from 10 mg to 20 mg were introduced in an aluminum capsule. They were first cooled to -80 °C and, after an isotherm of 1 min, a temperature ramp was applied (10 °C.min^{-1}) up to 150 °C. Then, an isotherm at 150 °C was applied for 1 min, and the temperature was decreased to -80 °C with a cooling rate of 10 °C.min^{-1}. This cycle was repeated twice. The glass transition temperature (T_g) was measured on the second cycle, with the TA *Universal Analysis* software, by drawing the tangents to the heat flow curve at temperatures above and below the glass transition. The accuracy on T_g is ± 4 °C.

Dynamic mechanical thermal analysis (DMTA) was carried out with a DMA3200 (TA Instruments) operating in tensile mode (strain: 0.05%, pre-tension: 0.01 N). The measurements were typically performed on 10 x 7 x 0.5 mm (length x width x thickness) samples at a frequency of 1 Hz and ranging from -80 °C to 150 °C (after a 1-minute isotherm at -80 °C) with a 3 °C.min^{-1} heating rate. The setup provided the storage and loss moduli (E' and E''). The damping parameter or loss factor (tan δ) was calculated as tan δ = E''/E'. Tα corresponds to the temperature where tan δ is maximum.

Thermogravimetric analysis (TGA) was performed using a NETZSCH STA 409 PC/PG. Samples with an average weight ca. 20 mg were placed in a platinum pan and heated from 30 °C to 900 °C at 10 °C.min^{-1}. Synthetic air with a flow rate of 60 mL.min^{-1} was used as the sweeping gas. The thermal stability of $SPE_{18.16}$ and si-$SPE_{21.16}$ was analyzed by TGA (Figure SI-1), they do not exhibit any degradation up to 200 °C which is highly satisfactory for electrolytes.

Electrochemical impedance spectroscopy (EIS) was carried out using a 1260 Solartron FRA device between 10^7 Hz and 10^{-1} Hz, with a perturbation of 100 mV at the open circuit voltage (OCV). The sample was assembled in a Swagelok-type cell using two stainless-steel blocking electrodes. The contact pressure was maintained with a spring (0.4 MPa). Data quality was evaluated using the Lin-KK Tool. [31–33] The distribution of relaxation time (DRT) analysis was performed using the MATLAB toolbox DRTtools.

To estimate the ionic conductivity of the samples, the intercept of the first semicircle in EIS measurements was considered to correspond to the bulk resistance (R_{bulk}) from which the conductivity was estimated ~~by~~ using the following relation:

$$\sigma = \frac{e}{R_{bulk} * S} \qquad \text{Equation 2}$$

where *e* is the thickness and *S* is the surface area of the sample. The measurement was carried out every 10 °C between 20 and 80 °C. The temperature was controlled using an environmental simulation chamber (Memmert). Cells were allowed to reach the thermal equilibrium for at least 1h before each test.

The Li transport number, the stability in potential and stripping plating measurements were carried out on a Biologic SP300 with a Swagelok-type cell. All ~~the~~ cells were assembled in glove box under argon (H_2O < 0.1 ppm). A Li-metal/polymer electrolyte/Li-metal cell was assembled and subjected to a 60 mV polarization bias (ΔV) to determine the initial ($i°$) and steady state (i^∞) currents. EIS was performed by applying a 100 mV perturbation between 10^6 Hz and 0.1 Hz at the OCV. The bulk resistance corresponds to the first semi-circle according to the characteristic frequencies. The values are ~ 10^6 Hz for SPE and ~10^4 Hz for si–SPE @ 25 °C (5x10^6 Hz for $SPE_{18,16}$ and 6x10^5 Hz for si-$SPE_{21,16}$ @ 80 °C)[16,21]. The bulk resistance was measured before (R^0_{bulk}) and after (R^∞_{bulk}) polarization. t_{Li+} was calculated using the following equation[17]:

$$t_{Li+} = \frac{i^\infty * R^\infty_{bulk} * (\Delta V - i^0 * R^0_{int})}{i^0 * R^0_{bulk} * (\Delta V - i^\infty * R^\infty_{int})} \qquad \text{Equation 3}$$

where the resistances before (R^0_{int}) and after polarization (R^∞_{int}) of the Li/polymer interface were measured at low frequency according to their characteristic frequencies (~ few Hz).

Cyclic voltammetry (CV) was used to determine the electrochemical stability window of the solid polymer electrolytes at 70 °C. The electrochemical cell was assembled by sandwiching polymer between the working electrode, and a metal Li foil as a reference and counter electrode, simultaneously. Stainless steel and copper were used as the working electrode during anodic and cathodic stability measurements, respectively. Potential scans were carried out between OCV and 7 V versus Li^+/Li at a constant scan rate of 1 $mV.s^{-1}$ to determine the anodic limit.

Galvanostatic cycling was employed to evaluate the critical current density (CCD). The symmetric cells were assembled in a Swagelok-type cell. The contact pressure of 0.4 MPa was maintained with a spring. First, the CCD value was estimated. To do so, the starting current density was 0.01 $mA.cm^{-2}$ and the current was subsequently increased up to 0.08 $mA.cm^{-2}$. An increase of the current by 0.04 $mA.cm^{-2}$ was then selected for each step. The plating and stripping were performed for 1h and separated by a rest period of 5 min, respectively. The measurement was stopped when the potential reached 4.5 V according to the working conditions of the cathode materials. After determining the CCD, the current density was fixed just below the CCD value, i.e. 0.2 $mA.cm^{-2}$ for si-$SPE_{21.16}$ and 0.12 $mA.cm^{-2}$ for $SPE_{18.16}$, for a period of 100 cycles of stripping and plating (200 h) to study the stability of the polymer against Li–metal electrode.

Li and TFSI diffusion coefficients were measured by NMR spectroscopy. Experiments were performed on a Bruker Av^{III} 300 spectrometer, operating at 116.64 MHz for ^7Li and 282.38 MHz for ^{19}F, equipped with a 5 mm BBFO probe (z gradient, G_{max}=49.7 $G.cm^{-1}$) or a 5 mm DIFF30 probe (z gradient, G_{max}=1200 $G.cm^{-1}$) associated to a $^7Li/^2D$ or $^{19}F/^2D$ insert. Measurements were made at 84° ± 1 °C on a stripe of polymer electrolytes (~20 x 4 x 0.3 mm^3), introduced in a 5 mm standard NMR tube. A pulsed field gradient stimulated spin echo sequence, with bipolar gradients and longitudinal eddy current delay (ledbpgp2s, from the Bruker standard library) was used. The eddy current delay was set to 5 ms and a smooth square shape (SMSQ10.100) was chosen for the gradient pulses. From 16 to 32 gradient values were used, ranging from 2% to 90% of the maximum gradient strength. The diffusion delay (D20) and the gradient pulse length (P30) were optimized for each sample and nucleus (^7Li or ^{19}F) in order to obtain an echo intensity below 10% at the strongest gradient, except for the ^{19}F measurements on the Si-$SPE_{21.16}$ sample in which TFSI is grafted to the polymer network ~~and~~ does not diffuse. Measures were performed with at least two different pairs of parameters (D20 and P30) to ensure reliability. The evolution of the echo intensity (or area) as a function of the gradient strength g was fitted with the standard Stejskal-Tanner formula to determine the diffusion coefficient D[34] :

$$\frac{I}{I_0} = \exp(-D(\gamma\delta g)^2\left(\Delta' - \frac{\delta}{3}\right)) \qquad \text{Equation 4}$$

where I_0 is the echo intensity at zero gradient, γ is the gyromagnetic ratio of the observed nucleus (^{7}Li or ^{19}F), δ the bipolar gradient pulse length (2*P30) and Δ' the corrected diffusion delay (D20+P30/24-D16/2, with D16 being the gradient recovery delay that was set at 0.2 ms).

The longitudinal (T_1) and transverse (T_2) relaxation times were measured with inversion recovery and cpmg pulse sequences, respectively.

3. Results and discussion

3.1. Single-ion solid polymer electrolytes polymer network synthesis

A series of single-ion solid polymer electrolytes (si–SPE) has been synthesized in an one-pot and solvent-free reaction from poly(ethylene glycol) methyl ether methacrylate (PEGM, M_n : 500 g.mol^{-1}), lithium 3-[(trifluoromethane)sulfonamidosulfonyl]propyl methacrylate (LiMTFSI) and poly(ethylene glycol) dimethacrylate (PEGDM, M_n : 750 g.mol^{-1}), used as crosslinker. Another series of solid polymer electrolytes (SPE) was obtained by replacing LiMTFSI monomer with LiTFSI salt. The free-radical polymerization of the methacrylate function was initiated by 2 wt% of 2,2′-azobis(2-methylpropionitrile) (AIBN) with respect to the monomers. A thermal curing of 2 h at 70 °C, followed by a post-curing of 1 h at 90 °C, was then applied.[35]. The synthetic scheme of (single-ion) solid polymer electrolytes is presented in Figure 1 and their composition as well as their main physico-chemical characteristics are summarized in Table 2. The obtained materials were self-standing and easy to handle in most cases. Depending on their composition, they change from flexible to hard and up to very brittle (Table 2).

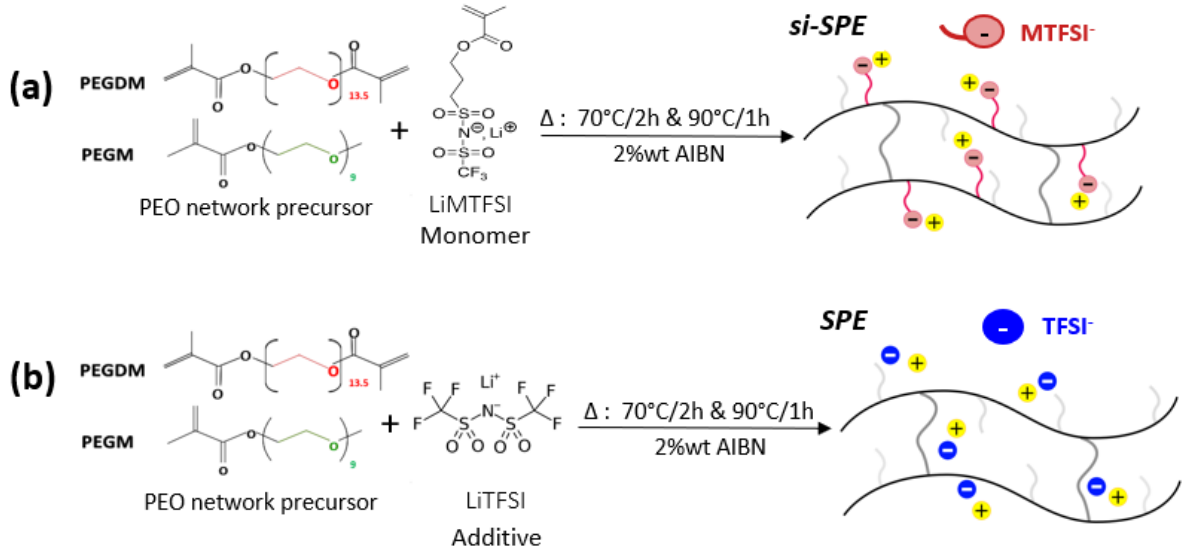

Figure 1. Synthesis scheme of (a) single-ion solid polymer electrolyte (si-SPE) and (b) solid polymer electrolyte (SPE).

First, the formation of the polymer networks for SPE and si−SPE samples was verified by the solid / liquid extraction with methanol, which can solubilize all precursors (Figure 2). Indeed, if the copolymerization is efficient, only LiTFSI salt can be removed from SPE. The pristine PEGM:PEGDM 80:20 network without Li monomer or Li salt, contained only 2 wt% of soluble fraction, attesting to the polymer network formation. As expected, the soluble fractions of the SPE samples increase linearly with the weight proportion of LiTFSI salt and they are only slightly higher than the quantity of LiTFSI salt introduced during the synthesis. This result indicates that the addition of LiTFSI into the PEO network precursor does not modify the formation of the PEO network.

On the other hand, the series of si-SPE synthesized from PEGM:PEGDM 80:20 mixture with different contents of LiMTFSI exhibits at most 6 wt% of soluble fraction (Figure 2), witnessing the efficient copolymerization of the different monomers: the Li-salts monomers (LiMTFSI) are grafted onto the polymer networks.

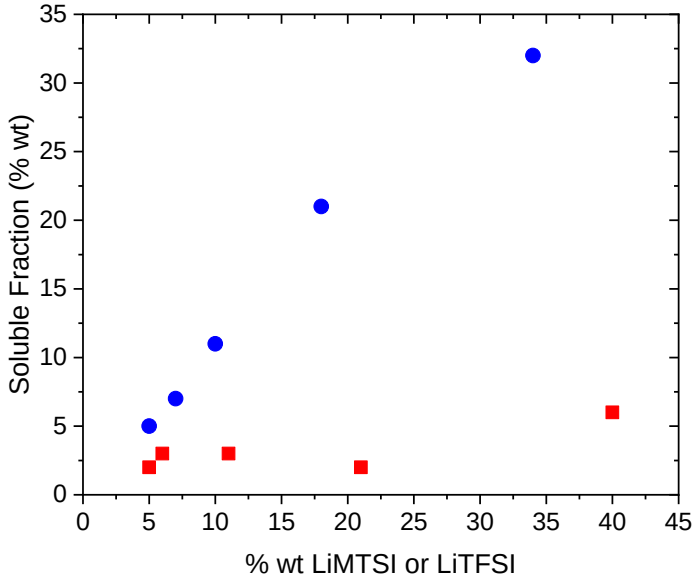

Figure 2. Soluble fractions of (si-SPEs) (■) and (SPEs) (●) versus the Li content added in the synthesis while keeping the same weight ratio of PEGM:PEGDM = 80:20.

The copolymerization efficiency was also approved by the absence of polymerization exotherm during the first DSC scan of resulting materials (Figure SI-2). Furthermore, the DSC analyses demonstrate the amorphous character of all the synthesized polymers since no crystallization exotherm was detected (Figure SI-3). T_g values of the different materials were determined from these DSC thermograms. While the pristine sample exhibits a T_g of -60 °C, the presence of only 5 wt% of Li-salt or Li monomer increases the T_g to -55 or -52 °C, respectively. This increase is linked to the strong interaction of the Li^+ to the PEO chains, as usually reported in the literature[2,36]. This effect is more remarkable with Li monomer, where the T_g reaches -29 °C at 40 wt% of MTFSI. Indeed, in the latter case, not only the interaction of Li/PEO chains occurs but also the introduction of ionic monomer (MTFSI) within the polymer network rigidifies the network itself, leading to a more pronounced increase in T_g. In addition, the T_g can also be

tuned by modulating the weight ratio between the PEGM:PEGDM, thus varying the crosslinking density (Table 2). Consequently, the T_g can be tuned to -31 °C for SPE and to -19 °C for si–SPE.

3.2. Ionic conduction properties

The ionic conductivity of different samples was measured at ambient temperature. The values range from 10^{-5} S.cm^{-1} to 10^{-8} S.cm^{-1}, depending on anionic grafting, the EO/Li ratio, and the cross-linking density. The change in ionic conductivity was then plotted as a function of T_g and is reported in Figure 3. It shows a linear relationship with T_g, irrespective of the Li concentration or the structure of the PEO polymer (linear or cross-linked). A slight deviation from a linear relationship is observed between grafted and ungrafted Li salts. It is important to note that during the conductivity measurements conducted at 25 °C, all samples are in the rubbery state due to their T_g being lower than -20 °C.

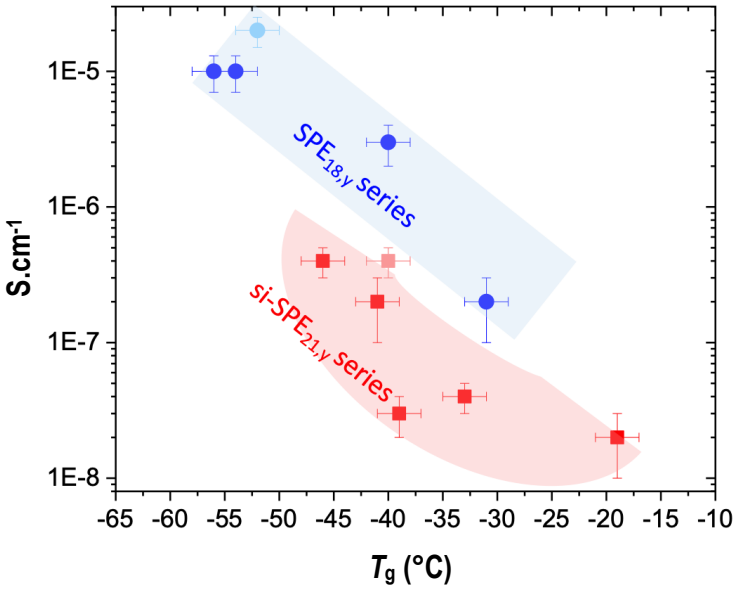

Figure 3. Ionic conductivity at 25 °C with respect to T_g for SPE$_{18,y}$ series (●) and si–SPE$_{21,y}$ series (■). Linear SPE (●) and linear si-SPE (■) correspond to the samples prepared without PEGDM.

To better understand the dependence of ionic conductivity with T_g, the different parameters (grafting of anionic moiety, cross-linking density, and EO/Li ratio) have been studied separately. First, for a similar T_g, the ionic conductivity is lower by about two orders of magnitude when the anionic moiety is grafted. For example, SPE$_{18.41}$ and si-SPE$_{21.40}$ (T_g around -40 °C) exhibit a conductivity of 3x10^{-6} and 3x10^{-8} S.cm^{-1}, respectively. Second, increasing the cross-linking density (PEGDM proportion) augments the T_g and induces an important impact on the ionic conductivity (see si-SPE$_{21.y}$ and SPE$_{18.y}$ series: Figure 3 and Table 1). For si-SPE, the highest conductivity value measured at 25 °C is as high as 4x10^{-7} S.cm^{-1} and is observed for the sample with the lowest content of cross-linker (si-SPE$_{21.4}$) and thus lowest T_g (–46°C). Note that the sample without a crosslinker exhibits the same conductivity but with a higher T_g (–40 °C). These results agree with Yu et al.[37] who showed for an electrolyte polymer that the lower ionic conductivity is observed for the higher cross–linking agent. Remarkably, the addition of more PEGDM

results in an increased crosslink density of the material, leading to a rise in the storage modulus, as observed in previous studies on different materials [38]. This modification makes the medium through which Li^+ must traverse more elastic and less viscous. To investigate this behavior, samples containing different proportions of PEGDM were analyzed by DMTA (Figure 4 and Figure SI-4).

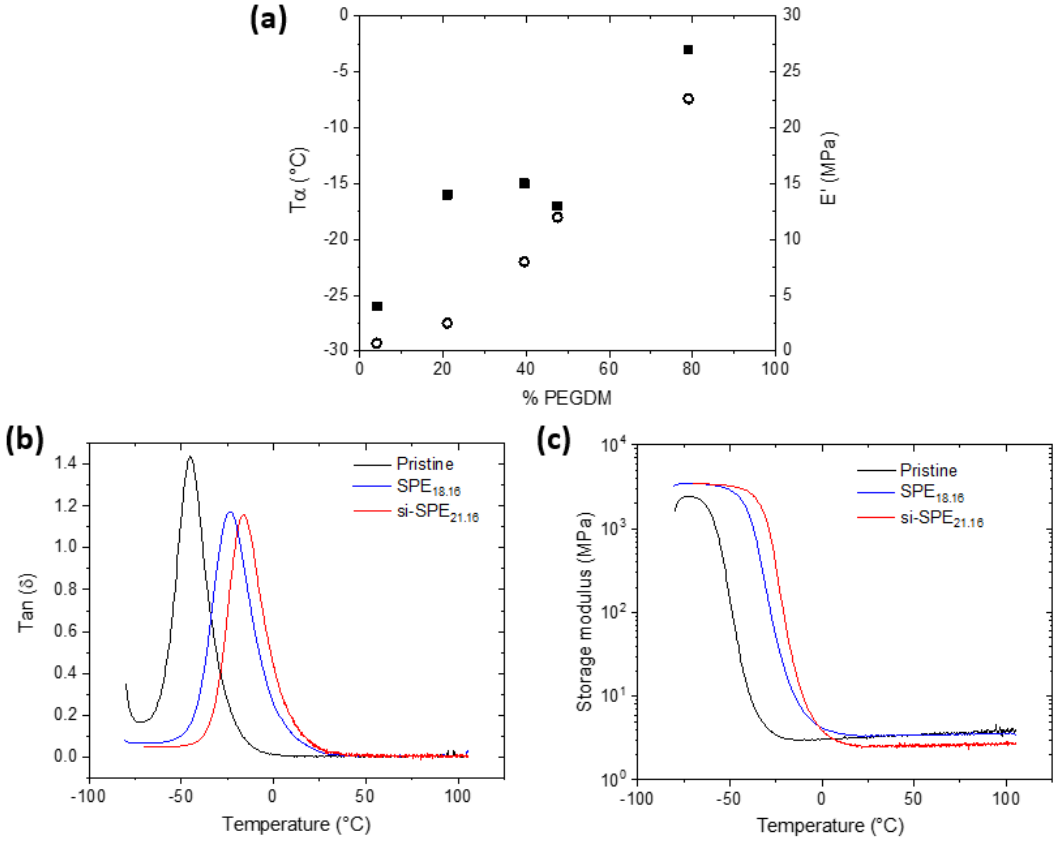

Figure 4. (a) Dynamic thermomechanical analysis storage modulus (E', O) and T_α (■) as function of PEGDM wt% for the si-$SPE_{21.y}$ samples; (b) tan(δ) versus T, and (c) storage modulus (E') vs. T for pristine network, si-$SPE_{21.16}$ and $SPE_{18.16}$ samples. The experiment has been repeated on three different samples with good reproducibility.

As expected, the storage modulus in the rubbery state (above 0 °C) increases from 1 to 20 MPa when the PEGDM proportion increases from 4 to 79 wt%. Simultaneously, the mechanical relaxation temperature T_α, measured at the maximum of the tanδ peak, increases from -26 for 4 wt% of PEGDM to -3 °C for 79 wt% of PEGDM.

Generally, PEO networks with grafted salts are not always homogeneous. To illustrate, when free-radical copolymerization is employed for PEGDM:PEGM with 2-acrylamido-2-methyl-1-propanesulfonic acid (AMPS), it results in materials that display phase separation[39]. To assess the homogeneity of LiMTFSI in the si-SPE samples, DMTA emerges as a valuable analytical tool. Indeed, DMTA often proves more sensitive than DSC when it comes to detecting phase separation. Consequently, the observation of a single peak in the α-relaxation associated with segmental chain

motions can be considered as a clear indicator of material homogeneity. The temperature-dependent tan δ of various si–$SPE_{21,y}$ samples exhibits a single peak (see Figure SI-4 (a)), affirming the absence of phase separation in the synthesized network[40]. Interestingly, it was found that the grafting of the anion (MTFSI) to the pristine polymer induces a significant rise of the α relaxation temperature (T_α) from -45 to -15 °C (Figure 4b) which is confirmed by a simultaneous increase of the T_g from -60 to -41 °C. The same effect was observed, yet to a lesser extent (shift of T_α from -45 to -23°C), on the $SPE_{18.16}$ sample, containing the same proportion of Li^+. The augmentation of T_α was related to the decrease of the mobility of the polymer chains upon the anion grafting to the polymer network as well as to the strong interaction of Li^+ with ethylene oxide units in the PEO chains[21].

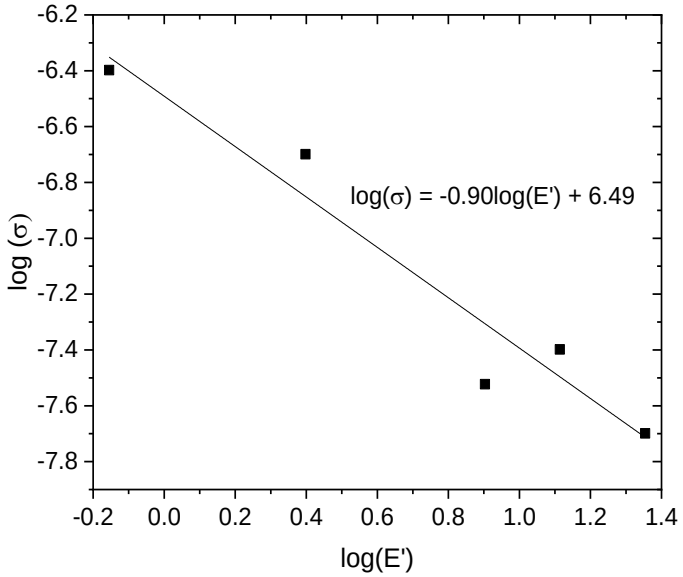

Figure 5. Logarithm conductivity of si-$SPE_{21.y}$ series as a function of the logarithm of its storage modulus at 25 °C.

Figure 5 represents the logarithm evolution of the ionic conductivity as a function of the logarithm of the storage modulus (E') for the si–$SPE_{21.y}$ series. It clearly shows that the ionic conductivity is inversely and strongly dependent on the storage modulus. This behavior is very similar to that of the well-known Walden rule relating the equivalent conductivity (Λ) of a liquid electrolyte to its viscosity (Λη = constant). The Walden rule has been extended to solid electrolyte by relating the conductivity to the structural (segmental) relaxation based on dielectric spectroscopic data[41]. In that case, the authors concluded that polyether–Lithium electrolytes (i.e., PEO–Li salt) exhibit a universal behavior in which ion and polymer dynamics are strongly coupled. To the best of our knowledge, the correlation between the viscoelastic properties of a solid and its storage modulus has not been previously established. In our case, the unique composition of the samples enables the meticulous control of critical parameters, such as ionic concentration and ethylene oxide content, by exclusively varying the modulus of the samples through adjustments in the PEGDM:PEGM ratio.

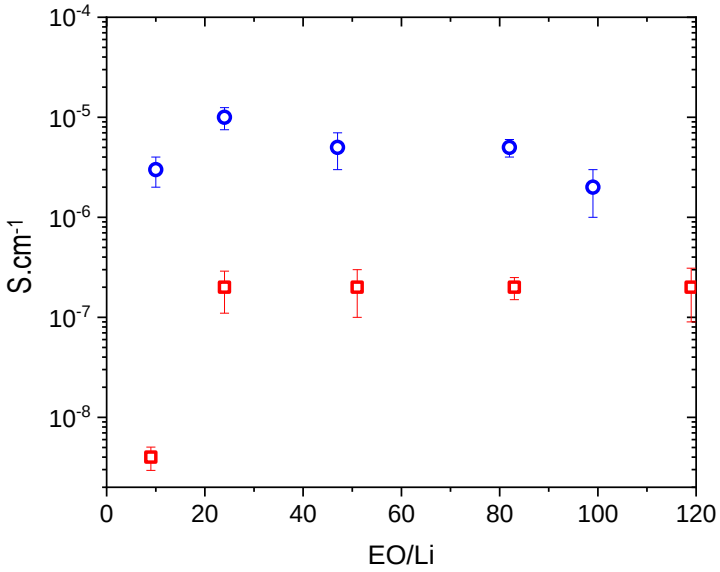

Figure 6. Variation of the ionic conductivity at 25 °C as function of EO/Li ratio for SPE (○) and si-SPE (□) electrolytes with a PEGM:PEGDM ratio of 80:20.

Subsequently, we investigated the correlation between conductivity and Li^+ concentration while keeping the PEGDM:PEGM ratio constant. Figure 6 depicts the variation in ionic conductivity of the polymer electrolytes as a function of the EO/Li ratio.

For both SPE and si-SPE electrolytes, the ionic conductivity increases with the EO/Li ratio, until it reaches *ca.* 20. For the SPE series, a maximum in conductivity is observed for an EO/Li ratio around 20, ~~value~~ similar to those reported in the literature for PEO/Li salt systems. For the si-SPE series, the conductivity stabilizes for higher ratios. Previously, a decrease of the conductivity was observed by Mindemark et al. for Li based SPE and by Bouchet et al.[2] for salt-grafted SPE when the EO/Li ratio increases. This behavior is usually attributed to a trade-off between the increase in charge carrier content, the increase in T_g, the crystallization of PEO, and the salt dissociation. For instance, Maurel *et al.* [43] have shown on PEO/LiTFSI samples an optimum in conductivity for an EO/Li ratio of 20. In our case, the EO/Li ratio has little effect on the conductivity. It is likely that at a high concentration of Li (low EO/Li), the high content of complex Li–EO induces an increase in the storage modulus of the material and therefore a simultaneous decrease of the conductivity happens, as shown previously (Figure 5). At lower concentrations (EO/Li above 20), the stabilization in conductivity in the case of si-SPE is a trade-off between the decrease in Li concentration and the increase in dissociation of Li-salt. On the contrary, the conductivity of SPE tends to decrease with the increase of the EO/Li ratio, due essentially to the decrease in salt concentration, as it is already highly dissociated. This issue will be further discussed in the following section, where we will subject si-$SPE_{21.16}$ and $SPE_{18.16}$ to different characterizations. These

two samples have been chosen because they share the same crosslink density and similar [EO]/[Li] ratios, but the anion is grafted onto si–$SPE_{21.16}$ while not on $SPE_{18.16}$.

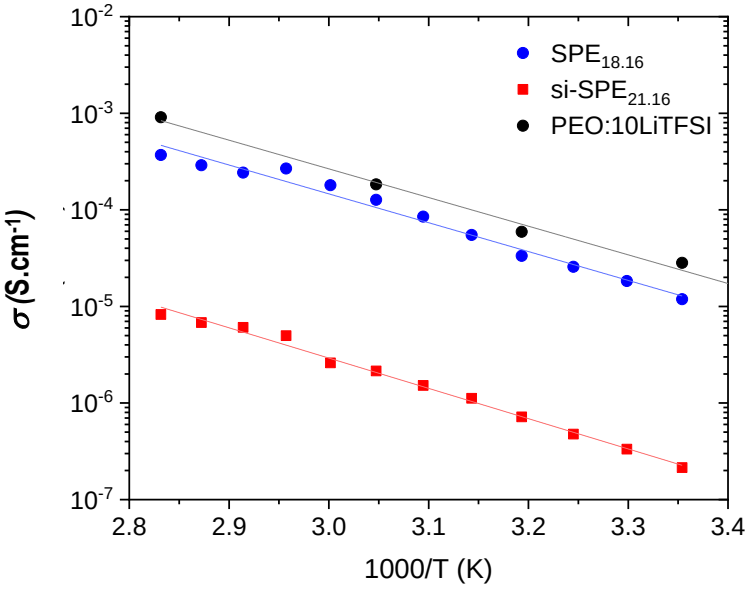

Figure 7. Arrhenius plot for $SPE_{18.16}$ EO/Li=24 (●) and si-$SPE_{21.16}$ EO/Li =24 (■)

The temperature dependence of the conductivity is depicted in Figure 7. The si-$SPE_{21.16}$ polymer electrolyte with immobilized anions has a notably lower ionic conductivity than $SPE_{18.16}$, which contains mobile anions, over the entire range of studied temperatures. Interestingly, the absence of any change in the slopes of the ln(σ) vs 1000/T plots (Figure 7) confirms that both polymer electrolytes do not undergo any crystallization process in the studied temperature range in agreement with the DSC results. The ionic conductivity of si-$SPE_{21.16}$ and $SPE_{18.16}$ follows Arrhenius model: $\sigma\ (T) = \sigma_0 * \exp(-\frac{E_a}{RT})$. From the plot of ln(σ) versus 1000/T, the activation energies (E_a) for $SPE_{18.16}$ and si–$SPE_{21.16}$ have been estimated at 0.64 eV and 0.62 eV, respectively. The similar E_a for both samples demonstrates that the Li^+ ions pathway along the polymer network obeys a similar diffusional mechanism. Compared to literature data on single ion polymer electrolytes[44], this higher activation energy value (0.62 eV compared to 0.22 eV) attests to a different mechanism of Li transport in our polymer matrix.

The Li ion transport numbers (t_{Li+}) of both $SPE_{18.16}$ and si-$SPE_{21.16}$ were estimated from the measurement of the diffusion coefficients of Li^+ and $TFSI^-$ measured by pulsed field gradient nuclear magnetic resonance (PFG-NMR) spectroscopy using the ^7Li or ^{19}F signals, which fall around 0 ppm and -78 ppm, respectively[45]. The diffusion coefficients determined at 84±1 °C for $SPE_{18.16}$ and si–$SPE_{21.16}$ are reported in Table 3. The primary reason for choosing to conduct the measurements at this temperature was that the relaxation times (T2) are too short at room temperature. However, at higher temperatures, relaxation times increase and become compatible with PFG-NMR.

The attenuation curve observed for the ^{19}F signal in si-$SPE_{21,16}$ (Figure SI-5a) shows almost no decay (~5%). It was yet fitted with 2 components to account for this weak decay. The major component corresponds to a diffusion coefficient that was set at $1x10^{-16}$ $m^2.s^{-1}$. It is associated to "immobile" species. The minor component corresponds to a diffusion coefficient of ~ $4x10^{-12}$ $m^2.s^{-1}$. This small amount of weakly mobile species could correspond to short oligomers or ends of chains.

The following relaxation times were observed for $SPE_{18.16}$: $T_1(^7Li)$=320 ms, $T_2(^7Li)$=120 ms, $T_1(^{19}F)$=1700 ms and $T_2(^{19}F)$=520 ms; and for si-$SPE_{21.16}$: $T_1(^7Li)$=280 ms, $T_2(^7Li)$=20 ms, $T_1(^{19}F)$=690 ms and $T_2(^{19}F)$=100 ms. In si-$SPE_{21.16}$, the T_2 is notably shorter, in line with a lower local mobility of the species. The transport numbers were then estimated with the following equation[46] :

$$t_{Li^+} = \frac{D_{Li}}{D_{Li} + D_{TFSI}}$$

where D_{Li} and D_{TFSI} represent the diffusion, coefficient measured in NMR spectroscopy for the Li and TFSI respectively. The obtained transport numbers are presented in Table 3.

Table 3. Diffusion coefficients at 84 °C, transport numbers and molar ionic conductivities of $SPE_{18.16}$ and si-$SPE_{21.16}$.

Sample	D_{Li} ($m^2.s^{-1}$)[a]	D_{TFSI} ($m^2.s^{-1}$)[b]	t^+_{NMR} (84°C)	t^+_{EI} (25°C)	[Li] (mol/L)	Λ_{NMR} ($\Omega^{-1}.m^2$)	Λ_{EIS} ($\Omega^{-1}.m^2$)[c]	α $\Lambda_{EIS}/\Lambda_{NMR}$
$SPE_{18,16}$	6.85×10^{-12}	1.54×10^{-11}	0.31	0.31	0.72	6.9×10^{-5}	5.8×10^{-5}	0.84
si–$SPE_{21,16}$	1.05×10^{-12}	$<1\times10^{-15}$	1.00	1.00	0.80	3.1×10^{-6}	2.1×10^{-6}	0.39

[a] uncertainty on D_{Li} is $\pm0.05x10^{-12}$ $m^2.s^{-1}$; [b] uncertainty on D_{TFSI} is $\pm0.02x10^{-11}$ $m^2.s^{-1}$ (but for si-$SPE_{21,16}$); [c] based on conductivity values measured at 80 °C

A value of 1.0 was obtained for si–$SPE_{21.16}$ and 0.31 for $SPE_{18.16}$. The t_{Li+} value was found to be 0.31 for $SPE_{18.16}$ at 25 °C. This low value, classically observed for PEO/Li salt electrolyte[13], indicates a limitation of Li^+ progression due to its coordination with the EO chains, while $TFSI^-$ is much less influenced[47,48]. For the si–$SPE_{21.16}$ sample, this value is equal to 1.00, confirming the total grafting of the LiMTFSI to the polymer network. This value is an excellent result as the t_{Li+} are generally reported to be close to unity (from 0.83 to 0.96) in most of single-ion conductors (cf Table SI-6). Interestingly, the main difference between the literature results and ours is the presence of solvent. In order to check this assumption, the si–$SPE_{21.16}$ sample was swollen with propylene carbonate until equilibrium. Once swollen, the t^+ of this sample decreases from 1 to 0.7, attesting the role of PC in the transport number of Li^+.[22]

We have also determined the Li ion transport number (t_{Li+}) of both $SPE_{18.16}$ and si–$SPE_{21.16}$ using the method proposed by Bruce and Vincent[49]. The results of EIS and polarization experiments are given in Figure SI-7. Surprisingly, the bulk resistance before and after polarization changes, indicating a modification of the concentration of Li in the PEO network or interfaces with Li metal. For these reasons, the Li ion transport number was estimated based on the NMR experiments.

Summarizing, the transport number value of 1.0 confirms that the ionic current in si–$SPE_{21.16}$ is exclusively due to Li^+ and their counter-ions (MTFSI) are covalently grafted to the polymer network (Table 3).

On the other hand, from diffusion coefficient, it is possible to calculate the molar ionic conductivity of the material using the Nernst–Einstein relation:

$$\Lambda_{NMR} = \frac{\sigma_{NMR}}{C} = \frac{N_A e^2}{kT}(D^+ + D^-)$$

with Avogadro's number (N_A), the fundamental charge (e), the Boltzmann constant (k) and the absolute temperature (T). These values can be compared with those obtained from EIS measurements, through the ratio $\Lambda_{EIS}/\Lambda_{NMR}$, which gives an indication on the proportion of charged species that contribute to ionic conduction. This ratio is considered as ionicity for ionic liquids or the degree of dissociation of liquid electrolytes[50,51]. Table 3 summarizes the diffusion coefficients and dissociation value (α) of both $SPE_{18.16}$ and si–$SPE_{21.16}$. In our case, the dissociation value of SPE is high, reaching 0.84 which is among the highest value reported in the literature even for liquid electrolytes ($\alpha < 0.8$ for $LiPF_6$ in PC or EC)[52,53]. This result is interesting as it suggests that the incorporation of the Li-salt within this network with dangling PEO chains allows keeping a high level of dissociation with a t^+ value similar to those obtained in the classical liquid electrolyte ($LiPF_6$/carbonate solvent $t^+ \sim 0.3 - 0.4$)[54]. The resulting low conductivity in our SPE case is mainly caused by the high viscosity/modulus of the medium, which is unavoidable due to the solid nature of the SPE. The dissociation value of si-SPE (0.39) is slightly higher than values reported in the literature for single-ion conducting solid polymer electrolyte (0.30)[55].

This feature has a considerable advantage over the ungrafted system due to their potential to reduce the build-up of ion concentration gradients, which is especially meaningful for fast charging applications,[54] and suppress Li dendrite growth,[56] which should improve the cycling stability and safety of the device.

The electrochemical stability window of $SPE_{18.16}$ and si–$SPE_{21.16}$ were investigated by cyclic voltammetry (CV) at 70 °C (Figure 8). Cathodic scans showed a couple of reversible redox peaks between -1.0 V and 7.0 V vs. Li at a scan rate of 1 $mV.s^{-1}$. The characteristic at the end of reduction at 0.0 V for si–$SPE_{21.16}$ and -0.5 V for $SPE_{18.16}$ was attributed to the Li deposition on the working electrode. The oxidation peak around 5.5 V for $SPE_{18.16}$ reflects the anodic stability of the electrolytes. The strong increase in current is probably associated with the decomposition of the anion as the anodic stability of the electrolyte is usually linked to the electrochemical stability of the anion[20]. The si–$SPE_{21.16}$ sample exhibits a slight increase of current at high potential, indicating an oxidation of the anion grafted to the polymer chains close to the electrode/electrolyte interface.

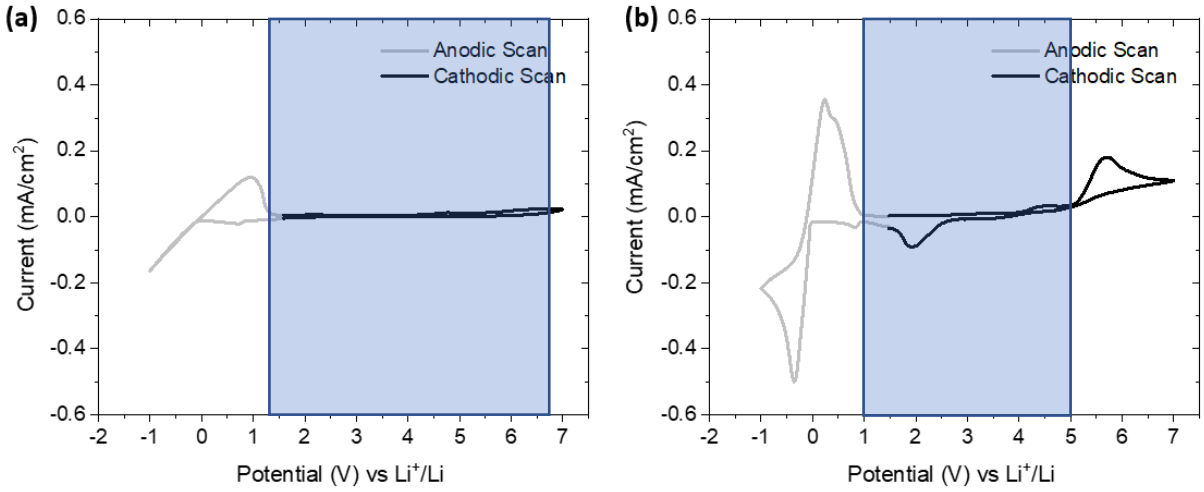

Figure 8. The electrochemical stability windows for (a) si–$SPE_{21.16}$ and (b) $SPE_{18.16}$ obtained by CV at 70 °C with a scan rate of 1mV.s^{-1}. **(**) Indicates the stability of the polymer vs Li–metal.

The increase in current for $SPE_{18.16}$ appears at a lower potential probably due to the presence of ungrafted anion in the polymer electrolyte. On the contrary for si–$SPE_{21.16}$, as the anions are grafted, anionic stability is postponed to higher potential values (7 V, in this cell configuration), as solely anions close to the interface can be oxidized[14]. These experiments confirm the importance of using the si–$SPE_{21.16}$ polymer in the formulation of composite positive electrodes with high potential cathode materials, due to its larger potential stability windows[57]. To our knowledge, High stability of single-ion SPE PEO based material has been reported by Bouchet et *al.*[8] work on P(STFSILi)-PEO-P(STFSILi), achieving a 6.5 V. Such high stability of si–$SPE_{21.16}$ could be explained by the grafting of the anion as well as the absence of solvent during the whole fabrication process[58].This high oxidation potential has recently shown by Xiong *et al.* [29] In particular, they show that high–concentration PEO solid electrolyte (EO:$Li^+ \leq 6.1$) is stable in oxidation potentials (≥5 V vs. Li/Li^+). This correlates with increasing the degree of coordinated EO.

In order to investigate the possibility of using these electrolytes in Li-metal batteries, the long-term electrochemical stability of both si–$SPE_{21.16}$ and $SPE_{18.16}$ against Li-metal was studied. To determine the appropriate applied current for cycling, we conducted tests with various currents to identify the one that did not lead to a polarization exceeding 4.5 V (Figure SI-8). This value was selected because it corresponds to the maximum working potential of the positive electrode. As a result, Symmetric Li/polymer electrolyte/Li cell was cycled at a constant current density of 0.2 mA.cm^{-2} for si–$SPE_{21.16}$ and 0.12 mA.cm^{-2} for $SPE_{18.16}$ at 70 °C (Figure 9). This current density has been determined according to the value measured in Figure SI-8. The voltage of the Li/ $SPE_{18.16}$/Li cell increases to 4.5 V after cycling for 266 h, while the voltage of the Li/si–$SPE_{21.16}$/Li reaches solely 1.5 V after 300 h of cycle. The increases of the polarization voltage may be attributed to a change in the Li concentration in the electrolyte. On the other hand, in contrast to the significant increase of the resistance for the

Li/$SPE_{18.16}$/Li cell from ~ $1.3x10^4$ Ω.cm to ~ $7.0x10^5$ Ω.cm (Figure 9d), the Li/si–$SPE_{21.16}$/Li cell showed a slight increase from ~ $2.3x10^5$ Ω.cm vs. ~ $2.8x10^5$ Ω.cm (Figure 9c), confirming the stability of the si–$SPE_{21.16}$ polymer/Li interface. Accordingly, the grafting of the anion to the network limits an overpotential in the cell, allowing a more stable system over time.

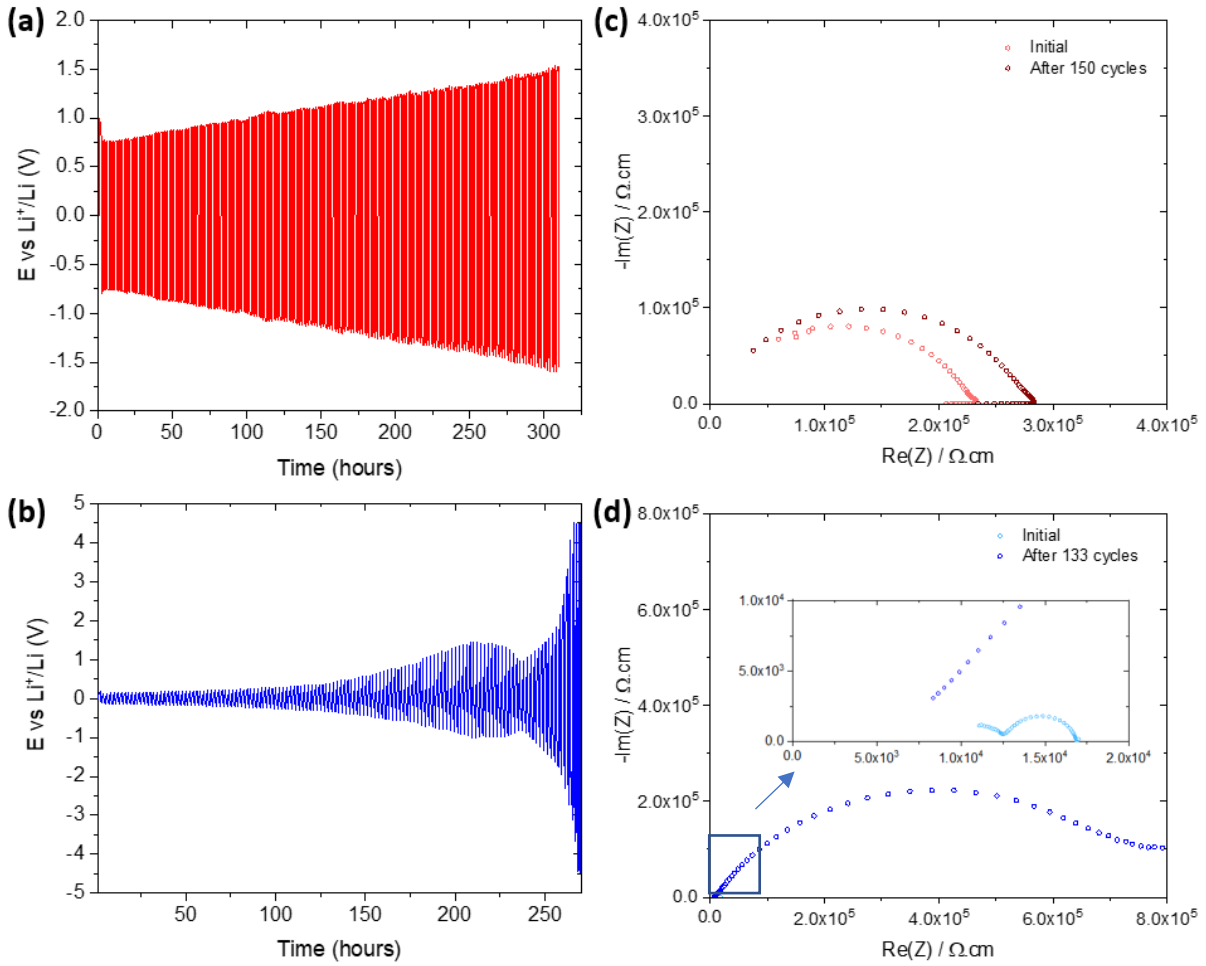

Figure 9. Galvanostatic cycling at 70 °C of (a)Li/si–$SPE_{21.16}$/Li at 0.2 $mA.cm^{-2}$ and (b) Li/$SPE_{18.16}$/Li 0.12 $mA.cm^{-2}$ and (c), (d) Nyquist plots of respective electrolyte before and after cycling. Both electrolytes have a thickness of 250 µm and an area of 0.5 cm^2.

4. Conclusion and perspectives

This study presents the synthesis and characterization of a series of cross–linked PEO polymers containing either grafted (si–$SPE_{x,y}$) or ungrafted ($SPE_{x,y}$) LiTFSI. The synthesis process involves a straightforward in-situ thermal copolymerization of commercial LiMTFSI, PEGM, and PEGDM without the use of solvents. Simultaneously, a crosslinked PEO polymer network was produced, incorporating dissolved LiTFSI salt. Flexible, self-supporting films of amorphous polymer electrolytes were prepared through thermal polymerization for 2 hours at 70 °C and 1 hour at 90 °C, allowing for easy variation of $SPE_{x,y}$ and single-ion conducting SPE (si–$SPE_{x,y}$) compositions. An analysis of the soluble fraction indicates successful copolymerization of the different monomers. DMTA and TGA

analyses confirm the homogeneity and thermal stability of the synthesized polymer films, respectively. Measurements of ionic conductivity, T_g (glass transition temperature), and E' (modulus) for various polymer electrolytes reveal a correlation between ionic conductivity and the mechanical properties (T_g and E') of the solid polymer film. The ionic conductivity (σ) decreases with the increase of T_g or T_α, particularly E', underscoring the role of PEO chain flexibility and the Li^+/PEO interaction on Li^+ transport within the PEO matrix. The unity value (1.00) of the transport number is obtained using diffusion coefficients in the case of si-SPE and electrochemical methods. Notably, si–$SPE_{21.16}$ exhibits robust mechanical properties, remaining self-standing over a wide temperature range (-70 °C to 100 °C, with a storage modulus of E' = 3 MPa at 25°C) and possessing a low T_g value of approximately – 40 °C. Its transport number of 1.0 is unprecedented in the available literature. Additionally, this material displays anionic stability at higher potential values (6 V). However, its ionic conductivity at ambient temperature, $2x10^{-7}$ $S.cm^{-1}$, is relatively low. To improve this value, changes in the PEO cross–linking chemistry are required to reduce the storage modulus of the material. The primary advantage of our Si–SPE and SPE polymers lies in their amorphous nature, in contrast to the majority of linear PEO polymers that exhibit semi-crystalline properties at room temperature. This amorphous characteristic enables their operation at ambient temperatures. It is worth noting that one of the major challenges in the development of all-solid-state batteries is achieving functionality at ambient temperatures

Supporting information:

TGA thermograms for SPE and si–SPE; DSC thermograms for si-SPE; DMA analysis for si–SPE; NMR experiments Attenuation curve for ^{19}F and ^{7}Li for SPE and si-SPE; Table of comparison of Li transport number; Determination of the Li transport numbers by Bruce et Vincent method, CCD determination at 70 °C for Li/SPE/Li and Li/si–SPE/Li.

Corresponding Authors

E-mail: christel.laberty@sorbonne-universite.fr
E-mail: tran-minh-giao.nguyen@cyu.fr

Acknowledgments

The authors thank RS2E network and DIM-Respore for supporting the PhD grants.

References:

(1) Lin, D.; Liu, Y.; Cui, Y. Reviving the Lithium Metal Anode for High-Energy Batteries. *Nat. Nanotechnol.* **2017**, *12* (3), 194–206. https://doi.org/10.1038/nnano.2017.16.
(2) Bouchet, R.; Maria, S.; Meziane, R.; Aboulaich, A.; Lienafa, L.; Bonnet, J.-P.; Phan, T. N. T.; Bertin, D.; Gigmes, D.; Devaux, D.; Denoyel, R.; Armand, M. Single-Ion BAB Triblock Copolymers as Highly Efficient Electrolytes for Lithium-Metal Batteries. *Nat. Mater.* **2013**, *12* (5), 452–457. https://doi.org/10.1038/nmat3602.

(3) Wang, Q.; Wang, H.; Wu, J.; Zhou, M.; Liu, W.; Zhou, H. Advanced Electrolyte Design for Stable Lithium Metal Anode: From Liquid to Solid. *Nano Energy* **2021**, *80*, 105516. https://doi.org/10.1016/j.nanoen.2020.105516.
(4) Li, M.; Wang, C.; Chen, Z.; Xu, K.; Lu, J. New Concepts in Electrolytes. *Chem. Rev.* **2020**, *120* (14), 6783–6819. https://doi.org/10.1021/acs.chemrev.9b00531.
(5) Mauger; Julien; Paolella; Armand; Zaghib. Building Better Batteries in the Solid State: A Review. *Materials* **2019**, *12* (23), 3892. https://doi.org/10.3390/ma12233892.
(6) Ma, Q.; Zhang, H.; Zhou, C.; Zheng, L.; Cheng, P.; Nie, J.; Feng, W.; Hu, Y.-S.; Li, H.; Huang, X.; Chen, L.; Armand, M.; Zhou, Z. Single Lithium-Ion Conducting Polymer Electrolytes Based on a Super-Delocalized Polyanion. *Angew. Chem. Int. Ed.* **2016**, *55* (7), 2521–2525. https://doi.org/10.1002/anie.201509299.
(7) Geiculescu, O. E.; Yang, J.; Zhou, S.; Shafer, G.; Xie, Y.; Albright, J.; Creager, S. E.; Pennington, W. T.; DesMarteau, D. D. Solid Polymer Electrolytes from Polyanionic Lithium Salts Based on the LiTFSI Anion Structure. *J. Electrochem. Soc.* **2004**, *151* (9), A1363. https://doi.org/10.1149/1.1773581.
(8) Tao, C.; Gao, M.-H.; Yin, B.-H.; Li, B.; Huang, Y.-P.; Xu, G.; Bao, J.-J. A Promising TPU/PEO Blend Polymer Electrolyte for All-Solid-State Lithium Ion Batteries. *Electrochimica Acta* **2017**, *257*, 31–39. https://doi.org/10.1016/j.electacta.2017.10.037.
(9) Marzantowicz, M.; Dygas, J. R.; Krok, F.; Łasińska, A.; Florjańczyk, Z.; Zygadło-Monikowska, E.; Affek, A. Crystallization and Melting of PEO:LiTFSI Polymer Electrolytes Investigated Simultaneously by Impedance Spectroscopy and Polarizing Microscopy. *Electrochimica Acta* **2005**, *50* (19), 3969–3977. https://doi.org/10.1016/j.electacta.2005.02.053.
(10) Kim, Y. The Effect of Plasticizers on Transport and Electrochemical Properties of PEO-Based Electrolytes for Lithium Rechargeable Batteries. *Solid State Ion.* **2002**, *149* (1–2), 29–37. https://doi.org/10.1016/S0167-2738(02)00130-3.
(11) Zheng, Q.; Pesko, D. M.; Savoie, B. M.; Timachova, K.; Hasan, A. L.; Smith, M. C.; Miller, T. F.; Coates, G. W.; Balsara, N. P. Optimizing Ion Transport in Polyether-Based Electrolytes for Lithium Batteries. *Macromolecules* **2018**, *51* (8), 2847–2858. https://doi.org/10.1021/acs.macromol.7b02706.
(12) Gao, K. W.; Loo, W. S.; Snyder, R. L.; Abel, B. A.; Choo, Y.; Lee, A.; Teixeira, S. C. M.; Garetz, B. A.; Coates, G. W.; Balsara, N. P. Miscible Polyether/Poly(Ether–Acetal) Electrolyte Blends. *Macromolecules* **2020**, *53* (14), 5728–5739. https://doi.org/10.1021/acs.macromol.0c00747.
(13) Devaux, D.; Bouchet, R.; Glé, D.; Denoyel, R. Mechanism of Ion Transport in PEO/LiTFSI Complexes: Effect of Temperature, Molecular Weight and End Groups. *Solid State Ion.* **2012**, *227*, 119–127. https://doi.org/10.1016/j.ssi.2012.09.020.
(14) Shi, Q.; Xue, L.; Qin, D.; Du, B.; Wang, J.; Chen, L. Single Ion Solid-State Composite Electrolytes with High Electrochemical Stability Based on a Poly(Perfluoroalkylsulfonyl)-Imide Ionene Polymer. *J Mater Chem A* **2014**, *2* (38), 15952–15957. https://doi.org/10.1039/C4TA02810D.
(15) Nguyen, N.; Blatt, M. P.; Kim, K.; Hallinan, D. T.; Kennemur, J. G. Investigating Miscibility and Lithium Ion Transport in Blends of Poly(Ethylene Oxide) with a Polyanion Containing Precisely-Spaced Delocalized Charges. *Polym. Chem.* **2022**, *13* (29), 4309–4323. https://doi.org/10.1039/D2PY00605G.
(16) Devaux, D.; Glé, D.; Phan, T. N. T.; Gigmes, D.; Giroud, E.; Deschamps, M.; Denoyel, R.; Bouchet, R. Optimization of Block Copolymer Electrolytes for Lithium Metal Batteries. *Chem. Mater.* **2015**, *27* (13), 4682–4692. https://doi.org/10.1021/acs.chemmater.5b01273.
(17) Feng, S.; Shi, D.; Liu, F.; Zheng, L.; Nie, J.; Feng, W.; Huang, X.; Armand, M.; Zhou,

Z. Single Lithium-Ion Conducting Polymer Electrolytes Based on Poly[(4-Styrenesulfonyl)(Trifluoromethanesulfonyl)Imide] Anions. *Electrochimica Acta* **2013**, *93*, 254–263. https://doi.org/10.1016/j.electacta.2013.01.119.
(18) Rolland, J.; Poggi, E.; Vlad, A.; Gohy, J.-F. Single-Ion Diblock Copolymers for Solid-State Polymer Electrolytes. *Polymer* **2015**, *68*, 344–352. https://doi.org/10.1016/j.polymer.2015.04.056.
(19) Inceoglu, S.; Rojas, A. A.; Devaux, D.; Chen, X. C.; Stone, G. M.; Balsara, N. P. Morphology–Conductivity Relationship of Single-Ion-Conducting Block Copolymer Electrolytes for Lithium Batteries. *ACS Macro Lett.* **2014**, *3* (6), 510–514. https://doi.org/10.1021/mz5001948.
(20) Porcarelli, L.; Shaplov, A. S.; Salsamendi, M.; Nair, J. R.; Vygodskii, Y. S.; Mecerreyes, D.; Gerbaldi, C. Single-Ion Block Copoly(Ionic Liquid)s as Electrolytes for All-Solid State Lithium Batteries. *ACS Appl. Mater. Interfaces* **2016**, *8* (16), 10350–10359. https://doi.org/10.1021/acsami.6b01973.
(21) Devaux, D. Comparison of Single-Ion-Conductor Block-Copolymer Electrolytes with Polystyrene-TFSI and Polymethacrylate-TFSI Structural Blocks. *Electrochimica Acta* **2018**, 12.
(22) Lechartier, M.; Porcarelli, L.; Zhu, H.; Forsyth, M.; Guéguen, A.; Castro, L.; Mecerreyes, D. Single-Ion Polymer/LLZO Hybrid Electrolytes with High Lithium Conductivity. *Mater. Adv.* **2022**, *3* (2), 1139–1151. https://doi.org/10.1039/D1MA00857A.
(23) Porcarelli, L.; Shaplov, A. S.; Bella, F.; Nair, J. R.; Mecerreyes, D.; Gerbaldi, C. Single-Ion Conducting Polymer Electrolytes for Lithium Metal Polymer Batteries That Operate at Ambient Temperature. *ACS Energy Lett.* **2016**, *1* (4), 678–682. https://doi.org/10.1021/acsenergylett.6b00216.
(24) Zhang, Y.; Cai, W.; Rohan, R.; Pan, M.; Liu, Y.; Liu, X.; Li, C.; Sun, Y.; Cheng, H. Toward Ambient Temperature Operation with All-Solid-State Lithium Metal Batteries with a Sp Boron-Based Solid Single Ion Conducting Polymer Electrolyte. *J. Power Sources* **2016**, *306*, 152–161. https://doi.org/10.1016/j.jpowsour.2015.12.010.
(25) Li, Z.; Guo, D.; Li, F.; Hou, G.; Liu, X.; Li, C.; Cao, L.; Wei, R.; Zhou, Z.; Lai, Z. Nerve Network-Inspired Solid Polymer Electrolytes (NN-SPE) for Fast and Single-Ion Lithium Conduction. *Energy Storage Mater.* **2022**, *49*, 575–582. https://doi.org/10.1016/j.ensm.2022.05.003.
(26) Niitani, T.; Shimada, M.; Kawamura, K.; Kanamura, K. Characteristics of New-Type Solid Polymer Electrolyte Controlling Nano-Structure. *J. Power Sources* **2005**, *146* (1–2), 386–390. https://doi.org/10.1016/j.jpowsour.2005.03.102.
(27) Sadoway, D. R. Block and Graft Copolymer Electrolytes for High-Performance, Solid-State, Lithium Batteries. *J. Power Sources* **2004**, *129* (1), 1–3. https://doi.org/10.1016/j.jpowsour.2003.11.016.
(28) Singh, M.; Odusanya, O.; Wilmes, G. M.; Eitouni, H. B.; Gomez, E. D.; Patel, A. J.; Chen, V. L.; Park, M. J.; Fragouli, P.; Iatrou, H.; Hadjichristidis, N.; Cookson, D.; Balsara, N. P. Effect of Molecular Weight on the Mechanical and Electrical Properties of Block Copolymer Electrolytes. *Macromolecules* **2007**, *40* (13), 4578–4585. https://doi.org/10.1021/ma0629541.
(29) Xiong, Z.; Wang, Z.; Zhou, W.; Liu, Q.; Wu, J.-F.; Liu, T.-H.; Xu, C.; Liu, J. 4.2V Polymer All-Solid-State Lithium Batteries Enabled by High-Concentration PEO Solid Electrolytes. *Energy Storage Mater.* **2023**, *57*, 171–179. https://doi.org/10.1016/j.ensm.2023.02.008.
(30) Wu, J.-F.; Yu, Z.-Y.; Wang, Q.; Guo, X. High Performance All-Solid-State Sodium Batteries Actualized by Polyethylene Oxide/Na2Zn2TeO6 Composite Solid Electrolytes. *Energy Storage Mater.* **2020**, *24*, 467–471. https://doi.org/10.1016/j.ensm.2019.07.012.

(31) Schönleber, M.; Klotz, D.; Ivers-Tiffée, E. A Method for Improving the Robustness of Linear Kramers-Kronig Validity Tests. *Electrochimica Acta* **2014**, *131*, 20–27. https://doi.org/10.1016/j.electacta.2014.01.034.
(32) Boukamp, B. A. A Linear Kronig-Kramers Transform Test for Immittance Data Validation. *J. Electrochem. Soc.* **1995**, *142* (6), 1885–1894. https://doi.org/10.1149/1.2044210.
(33) Schönleber, M.; Ivers-Tiffée, E. Approximability of Impedance Spectra by RC Elements and Implications for Impedance Analysis. *Electrochem. Commun.* **2015**, *58*, 15–19. https://doi.org/10.1016/j.elecom.2015.05.018.
(34) Grosso, D.; Ribot, F.; Boissiere, C.; Sanchez, C. Molecular and Supramolecular Dynamics of Hybrid Organic–Inorganic Interfaces for the Rational Construction of Advanced Hybrid Nanomaterials. *Chem Soc Rev* **2011**, *40* (2), 829–848. https://doi.org/10.1039/C0CS00039F.
(35) Dagousset, L.; Pognon, G.; Nguyen, G. T. M.; Vidal, F.; Jus, S.; Aubert, P.-H. Self-Standing Gel Polymer Electrolyte for Improving Supercapacitor Thermal and Electrochemical Stability. *J. Power Sources* **2018**, *391*, 86–93. https://doi.org/10.1016/j.jpowsour.2018.04.073.
(36) Gauthier, C.; Plesse, C.; Vidal, F.; Pelletier, J.-M.; Chevrot, C.; Teyssié, D. Polybutadiene/Poly(Ethylene Oxide) Based IPNs, Part II: Mechanical Modelling and LiClO4 Loading as Tools for IPN Morphology Investigation. *Polymer* **2007**, *48* (26), 7476–7483. https://doi.org/10.1016/j.polymer.2007.10.035.
(37) Yu, X.; Xiao, M.; Wang, S.; Han, D.; Meng, Y. Fabrication and Properties of Crosslinked Poly(Propylene Carbonate Maleate) Gel Polymer Electrolyte for Lithium-Ion Battery. *J. Appl. Polym. Sci.* **2010**, n/a-n/a. https://doi.org/10.1002/app.32480.
(38) Berrebi, M.; Fabre-Francke, I.; Lavédrine, B.; Fichet, O. Development of Organic Glass Using Interpenetrating Polymer Networks with Enhanced Resistance towards Scratches and Solvents. *Eur. Polym. J.* **2015**, *63*, 132–140. https://doi.org/10.1016/j.eurpolymj.2014.12.010.
(39) Chikh, L.; Girard, S.; Teyssie, D.; Fichet, O. Proton Conducting PAMPS Networks: From Flexible to Rigid Materials. *J. Appl. Polym. Sci.* **2008**, *107* (6), 3672–3680. https://doi.org/10.1002/app.27471.
(40) Szczepanski, C. R.; Pfeifer, C. S.; Stansbury, J. W. A New Approach to Network Heterogeneity: Polymerization Induced Phase Separation in Photo-Initiated, Free-Radical Methacrylic Systems. *Polymer* **2012**, *53* (21), 4694–4701. https://doi.org/10.1016/j.polymer.2012.08.010.
(41) Wang, Y.; Fan, F.; Agapov, A. L.; Yu, X.; Hong, K.; Mays, J.; Sokolov, A. P. Design of Superionic Polymers—New Insights from Walden Plot Analysis. *Solid State Ion.* **2014**, *262*, 782–784. https://doi.org/10.1016/j.ssi.2013.09.026.
(42) Mindemark, J.; Lacey, M. J.; Bowden, T.; Brandell, D. Beyond PEO—Alternative Host Materials for Li + -Conducting Solid Polymer Electrolytes. *Prog. Polym. Sci.* **2018**, *81*, 114–143. https://doi.org/10.1016/j.progpolymsci.2017.12.004.
(43) Maurel, A.; Armand, M.; Grugeon, S.; Fleutot, B.; Davoisne, C.; Tortajada, H.; Courty, M.; Panier, S.; Dupont, L. Poly(Ethylene Oxide)−LiTFSI Solid Polymer Electrolyte Filaments for Fused Deposition Modeling Three-Dimensional Printing. *J. Electrochem. Soc.* **2020**, *167* (7), 070536. https://doi.org/10.1149/1945-7111/ab7c38.
(44) Ahmed, F.; Choi, I.; Rahman, Md. M.; Jang, H.; Ryu, T.; Yoon, S.; Jin, L.; Jin, Y.; Kim, W. Remarkable Conductivity of a Self-Healing Single-Ion Conducting Polymer Electrolyte, Poly(Ethylene- *Co* -Acrylic Lithium (Fluoro Sulfonyl)Imide), for All-Solid-State Li-Ion Batteries. *ACS Appl. Mater. Interfaces* **2019**, *11* (38), 34930–34938. https://doi.org/10.1021/acsami.9b10474.

(45) Hayamizu, K.; Seki, S.; Haishi, T. Lithium Ion Micrometer Diffusion in a Garnet-Type Cubic Li $_7$ La $_3$ Zr $_2$ O $_{12}$ (LLZO) Studied Using ^{7} Li NMR Spectroscopy. *J. Chem. Phys.* **2017**, *146* (2), 024701. https://doi.org/10.1063/1.4973827.
(46) Zhao, J.; Wang, L.; He, X.; Wan, C.; Jiang, C. Determination of Lithium-Ion Transference Numbers in LiPF[Sub 6]–PC Solutions Based on Electrochemical Polarization and NMR Measurements. *J. Electrochem. Soc.* **2008**, *155* (4), A292. https://doi.org/10.1149/1.2837832.
(47) Oradd, G. Diffusion: A Comparison between Liquid and Solid Polymer LiTFSI Electrolytes. *Solid State Ion.* **2002**, *152–153*, 131–136. https://doi.org/10.1016/S0167-2738(02)00364-8.
(48) Edman, L.; Ferry, A.; Orädd, G. Analysis of Diffusion in a Solid Polymer Electrolyte in the Context of a Phase-Separated System. *Phys. Rev. E* **2002**, *65* (4), 042803. https://doi.org/10.1103/PhysRevE.65.042803.
(49) Bruce, P. Conductivity and Transference Number Measurements on Polymer Electrolytes. *Solid State Ion.* **1988**, *28–30*, 918–922. https://doi.org/10.1016/0167-2738(88)90304-9.
(50) Tokuda, H.; Hayamizu, K.; Ishii, K.; Susan, Md. A. B. H.; Watanabe, M. Physicochemical Properties and Structures of Room Temperature Ionic Liquids. 2. Variation of Alkyl Chain Length in Imidazolium Cation. *J. Phys. Chem. B* **2005**, *109* (13), 6103–6110. https://doi.org/10.1021/jp044626d.
(51) MacFarlane, D. R.; Forsyth, M.; Izgorodina, E. I.; Abbott, A. P.; Annat, G.; Fraser, K. On the Concept of Ionicity in Ionic Liquids. *Phys. Chem. Chem. Phys.* **2009**, *11* (25), 4962. https://doi.org/10.1039/b900201d.
(52) Feng, Z.; Higa, K.; Han, K. S.; Srinivasan, V. Evaluating Transport Properties and Ionic Dissociation of LiPF $_6$ in Concentrated Electrolyte. *J. Electrochem. Soc.* **2017**, *164* (12), A2434–A2440. https://doi.org/10.1149/2.0941712jes.
(53) Hayamizu, K. Temperature Dependence of Self-Diffusion Coefficients of Ions and Solvents in Ethylene Carbonate, Propylene Carbonate, and Diethyl Carbonate Single Solutions and Ethylene Carbonate + Diethyl Carbonate Binary Solutions of LiPF $_6$ Studied by NMR. *J. Chem. Eng. Data* **2012**, *57* (7), 2012–2017. https://doi.org/10.1021/je3003089.
(54) Diederichsen, K. M.; McShane, E. J.; McCloskey, B. D. Promising Routes to a High Li $^+$ Transference Number Electrolyte for Lithium Ion Batteries. *ACS Energy Lett.* **2017**, *2* (11), 2563–2575. https://doi.org/10.1021/acsenergylett.7b00792.
(55) Borzutzki, K.; Thienenkamp, J.; Diehl, M.; Winter, M.; Brunklaus, G. Fluorinated Polysulfonamide Based Single Ion Conducting Room Temperature Applicable Gel-Type Polymer Electrolytes for Lithium Ion Batteries. *J. Mater. Chem. A* **2019**, *7* (1), 188–201. https://doi.org/10.1039/C8TA08391F.
(56) Ford, H. O.; Park, B.; Jiang, J.; Seidler, M. E.; Schaefer, J. L. Enhanced Li $^+$ Conduction within Single-Ion Conducting Polymer Gel Electrolytes via Reduced Cation–Polymer Interaction. *ACS Mater. Lett.* **2020**, *2* (3), 272–279. https://doi.org/10.1021/acsmaterialslett.9b00510.
(57) Armand, M.; Tarascon, J.-M. Building Better Batteries. *Nature* **2008**, *451* (7179), 652–657. https://doi.org/10.1038/451652a.
(58) Nguyen, H.-D.; Kim, G.-T.; Shi, J.; Paillard, E.; Judeinstein, P.; Lyonnard, S.; Bresser, D.; Iojoiu, C. Nanostructured Multi-Block Copolymer Single-Ion Conductors for Safer High-Performance Lithium Batteries. *Energy Environ. Sci.* **2018**, *11* (11), 3298–3309. https://doi.org/10.1039/C8EE02093K.

TOC :

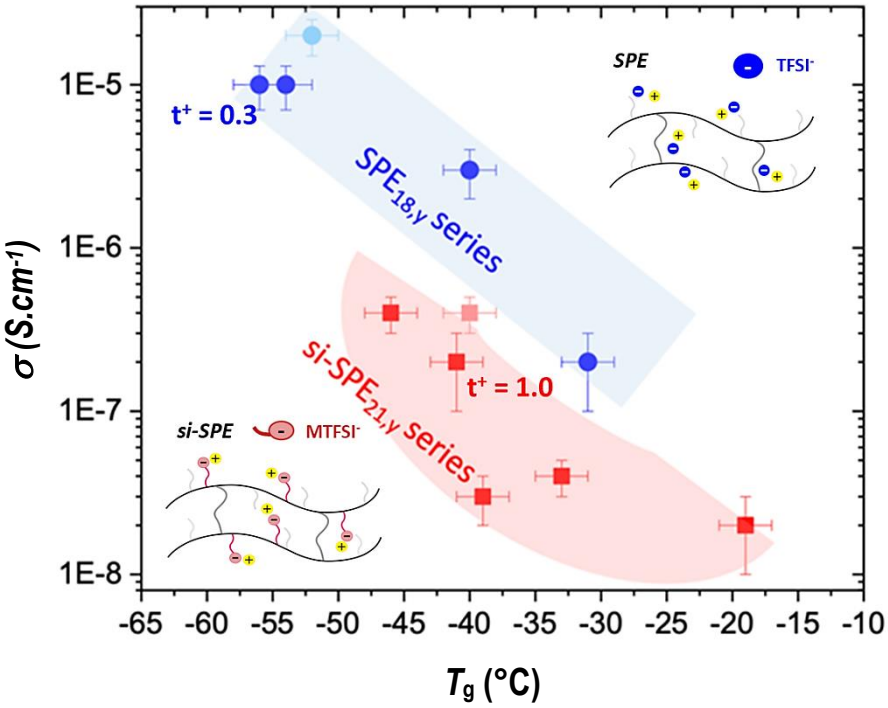
1E-5
1E-6
1E-7
1E-8
σ (S.cm-1)
-65 -60 -55 -50 -45 -40 -35 -30 -25 -20 -15 -10
Tg (°C)
t+ = 0.3
SPE18,y series
SPE
TFSI-
si-SPE21,y series
t+ = 1.0
si-SPE
MTFSI-